International Journal of Biological Macromolecules 138 (2019) 744–754

Contents lists available at ScienceDirect

International Journal of Biological Macromolecules

journal homepage: http://www.elsevier.com/locate/ijbiomac

Paper based immunosensing of ovarian cancer tumor protein CA 125 using novel nano-ink: A new platform for efficient diagnosis of cancer and biomedical analysis using microfluidic paper-based analytical devices (μPAD)

Farnas Bahavarnia [a], Arezoo Saadati [a,1], Soodabeh Hassanpour [a], Mohammad Hasanzadeh [b,*], Nasrin Shadjou [c], Ahmad Hassanzadeh [d]

[a] Pharmaceutical Analysis Research Center, Tabriz University of Medical Sciences, Tabriz, Iran
[b] Drug Applied Research Center, Tabriz University of Medical Sciences, Tabriz 51664, Iran
[c] Nanotechnology Research Center, Urmia University, Urmia, Iran
[d] Department of Processing, Helmholtz-Institute Freiberg for Resource Technology, Helmholtz-Zentrum Dresden-Rossendorf, Chemnitzer Str. 40, 09599 Freiberg, Germany

ARTICLE INFO

Article history:
Received 18 May 2019
Received in revised form 4 July 2019
Accepted 17 July 2019
Available online 18 July 2019

Keywords:
Tumor protein
Biosensor
Ovarian cancer
Nanomaterial
Bioanalysis

ABSTRACT

Ovarian cancer is the first and most important cause of malignancy death in women. Mucin 16 or MUC16 protein also known as carcinoma antigen 125 (CA 125) is the most commonly used glycoprotein for early stage diagnosis of ovarian cancer. In this work, a novel paper-based bio-device through hand writing of Ag/RGO (silver nanoparticles/reduced graphene oxide) nano-ink on the flexible paper substrate using pen-on-paper technology was developed. The prepared interface was used to the recognition of CA 125 protein in human biofluid. For this purpose, Ag/rGO nano-ink was synthesized by deposition of Ag nanoparticles onto graphene oxide sheets and the reduction of graphene oxide to rGO simultaneously. Conductivity and resistance of conductive lines were studied after drawing on photographic paper. Subsequently, to prepare a new and unique immuno-device, paper electrode modified by cysteamine caped gold nanoparticles (CysA/Au NPs) using electrochemical techniques. CysA is bonded by sulfur atoms with Au (CysA/Au NPs), and from the amine group with hydroxyl and carboxyl groups of Ag/RGO nano-ink deposited on the surface of paper-based electrodes (CysA/Au NPs/Ag-rGO). Then, anti-CA 125 antibody was immobilized on the electrode surface through Au NPs and CA 125 positively charged amine groups interaction. Atomic force microscopy, Transmission electron microscopy, Field emission scanning electron microscopy, and dynamic light scattering, were performed to identify the engineered immunosensor. Using chronoamperometry technique and under the optimized conditions, the low limit of quantitation (LLOQ) for the proposed immunoassay was recorded as 0.78 U/ml, which this evaluation was performed at highly linear range of 0.78–400 U/ml. The high sensitivity of the electrochemical immunosensor device is indicative of the ability of this immuno-device to detect early stages ovarian cancer.

1. Introduction

Ovarian cancer is the first and most important cause of malignancy death in women with more than 151,000 people per year [1]. Over the past decades, despite the development of chemotherapy and radical surgery, there has been no significant improvement in the survival rates of ovarian cancer patients [2], and screening studies have not been successful for the past 30 years. According to studies, some of the screened cases show a significant mortality rate that has been subject to inessential surgery as a result of faulty positive tests [3].

Biomarkers are used as a measurable indicator to evaluate some of the biological conditions, biological processes, and pathogenic processes or drug responses [4]. Therefore, a biomarker represents a change in expression, or a change in the state of a protein associated with a specific disease. CA. 125 (cancer-associated antigen-125), which plays an important role in increasing the proliferation of cancer cells and inhibition of anticancer immune response, is widely used as a dedicated serum marker for the detection of ovarian cancer [5]. The CA.125 was first discovered by Bast Knapp in 1981 [6,7] and has an O-linked glycoprotein. Concentrations higher than 35 of the MUC16 (Mucin 16 or CA 125) in blood (ordinarily less than 35 U/ml) associated with ovarian carcinoma and its progress [8–10]. To date, various methods have been developed,

* Corresponding author.
E-mail addresses: hasanzadehm@tbzmed.ac.ir, mhmmd_hasanzadeh@yahoo.com (M. Hasanzadeh).
[1] Co-first author: Equal contribution.

https://doi.org/10.1016/j.ijbiomac.2019.07.109
0141-8130/

such as enzyme-linked immuno-sorbent assay (ELISA) [11], solid-phase sandwich enzyme immunoassay [12] and electrochemical immunosensor [13–15] for the diagnosis of CA 125. Regardless, the conventional methods are expensive and time consuming and require experienced staff. Therefore, electrochemical immunosensor has been widely used in the diagnosis of cancer biomarkers due to their high sensitivity and specificity and low cost [16–18].

Immunosensor is a device that can detect antibody-antigen binding, but antigen and antibody interaction alone is not enough to produce a sensitive electrochemical signal. Hence, the use of various nanomaterials (e.g., noble metal NPs, metal nitride NPs, metal oxides NPs and carbon-based NPs) has been developed to improve the electrode abilities, including sensitivity, stability and electrical conductivity, as well as the improvement of the performance of electrochemical biosensors [19–22]. Among metal nanoparticles, gold nanoparticles (AuNPs) due to biocompatibility and stability, electrochemical, optical, electromagnetic and catalytic features have been extensively used in biosensing [23,24]. Taking into account the reported works, thiol is one of the most suitable functional group employed for linking to metals through formation of potent and strong sulfur-metal bond. It is noted that Cysteamine (CysA), a type of biomolecule containing sulfur, is usually applied as the Au NPs stabilizer and as an attachment agent at surface of Au NPs [25].

Although ordinary immunoassay methods are highly sensitive and widely used in many areas, they require different stages of preparation, skilled technicians and expensive equipment [26,27]. Hence, paper-based immunoassays have been advanced to address the above mentioned needs and have attracted the attention of many researchers [28]. Paper is used as the main ingredient in the provision of paper-based immunoassay devices, which are considered as ubiquitous, inexpensive, easy manipulation, tools-free, and disposable [29]. The valuable features of paper can be noted in the abundance, biodegradability, availability, light weight, and also the ability to pass liquid materials through its hydrophilic matrix without the need for external force [30]. Due to its fibrous porous structure, paper can drive aqueous liquid flows by capillary force and provides a large surface for reagents immobilization and a big zone for reagents reactions. The paper has a fibrous porous structure and is capable of directing aqueous fluid flow through the capillary force. Also, paper can provide a large surface for the immobilization and interaction of reagents [28].

In recent years, production of conductive patterns on paper as low-cost substrates has been considered as a simple method for designing paper-based sensors [31]. Due to the possibility of low-cost and quick screening as well as the design of customized electrodes, paper-based sensors are a good alternative to ordinary electrochemical sensors [32]. On the other hands, the pen-on-paper model provides a peculiar application for the fabricating flexible instruments by using a patterning device that is itself as universal and easily carried as the paper substrate. Rollerball pens are remarkably suited for distributing conductive bio-inks due to their agreement with gels and liquids [33].

Considering the significance of conductive nano-inks in construction of electrochemical biosensors for early and easy detection of cancer, both the public and private sector are ready to utilize this new technology. Due to the necessity of health centers such as research centers, hospitals, medical clinics, medical services, clinical laboratories for the early stage diagnosis of ovarian cancer, these centers have urgent necessity for these kind of nano-biosensors.

Therefore the purpose of the present study is to prepare a first novel paper-based immunosensor based on Ag/RGO conductive nano-ink for detection of ovarian cancer biomarker (CA 125) and early stage diagnosis of ovarian cancer. To do this, Ag/RGO nano-ink was synthesized by deposition of Ag nanoparticles onto graphene oxide sheets and the reduction of graphene oxide to RGO simultaneously. Conductivity and resistance of conductive lines were studied after drawing on photographic paper. Subsequently, to prepare a new and unique immunosensor, paper electrode prepared using CysA/Au NPs was modified electrochemically. Cys A is bonded by sulfur atoms with Au (CysA/Au NPs), and from the amine group with hydroxyl and carboxyl groups of Ag/RGO nano-ink deposited on the surface of paper-based electrodes (CysA/Au NPs/Ag-RGO). Then, the anti-CA 125 antibody was immobilized on the electrode surface through Au NPs and CA 125 positively charged amine groups interaction. Tests AFM (Atomic force microscopy), TEM (Transmission electron microscopy), FE-SEM (Field emission scanning electron microscopy), EDS, and DLS (dynamic light scattering), were performed to identify the engineered immunosensor. The chronoamperometry (ChA) technique was also used to detect CA 125 biomarker. The high sensitivity of the electrochemical immunosensor device is indicative of the ability of this immunodevice to detect early stages ovarian cancer.

2. Materials and methods

2.1. Chemical and reagents

NHS (N-hydroxysuccinimide), EDC (1-ethyl-3-(3-dimethylaminopropyl) carbodiimide hydrochloride), BSA (bovine serum albumin), PVP (Polyvinyl pyrrolidone) K-30 (molecule weight ≈300 g), disodium hydrogen orthophosphate, sodium hydroxide, Cysteamine hydrochloride, EG (ethylene glycol), sodium citrate, potassium ferricyanide $K_3Fe(CN)_6$, potassium dihydrogen orthophosphate, hydrogen tetrachloroaurate (III) hydrate ($HAuCl_4.3H_2O$), potassium ferrocyanide $K_4Fe(CN)_6$, ethanol, and potassium chloride were obtained from Sigma Aldrich (Ontario, Canada). $AgNO_3$ was obtained from Sigma Aldrich. 0.1 M, pH ~7.4 PBS (phosphate buffer saline) solution was prepared by dissolving 0.2 M Na_2HPO_4 and 0.2 M NaH_2PO_4 in deionized water (DW). Human CA-125 ELISA kit (CanAg/CA-125 EIA) involving CA-125 antigen, dilute solutions, ABC (avidin biotin-peroxidase complex), biotinilated solution, antibody (HRP Labeled anti-CA-125) standard, and standard buffer were purchased from CanAg Diagonestic AB Technology Co., (Gotenberg, Sweden). Human plasma samples were obtained from the Iranian Blood Transfusion Research Center (Tabriz, Iran).

2.2. Apparatus

Electrochemical processes were carried out with a PalmSens 4c system, driven with PSTrace5 software. The equilibrium time was 2 s and the employed ac voltage amplitude was 10 mV. Pt wire was applied as a counter electrode and Ag/AgCl (Metrohm, The Netherlands) as a reference electrode. Ag/RGO paper electrode which synthesized and prepared by ourselves was applied as a working electrode.

FE-SEM (high-resolution field emission scanning electron microscope), Hitachi SU8020, Czech with an operating voltage of 3 kV was applied for characterization of electrode surface morphology, and EDS (energy dispersive spectroscopy) coupled with the FE-SEM apparatus was applied for analysis of electrode chemical compositions. TEM (transmission electron microscopy), Adelaide, Australia with an operating voltage of 200 kV was applied for investigation of synthesis mechanism. Size distribution and zeta potential of Ag/RGO nano-ink was analyzed by DLS (dynamic light scattering) with zeta potential instrument Malvern Instruments Ltd. (Zetasizer Ver. 7.11, MAL1032660, England). Ohmmeter, XIOLE, XL830L, China, multi-meter was applied for resistivity and conductivity nano-ink estimate.

2.3. Synthesis of CysA-Au NPs

Briefly, 50 ml of $HAuCl_4$ (0.5 mM) was magnetically stirred and heated until 100 °C under reflux states. Later, 5 ml of $Na_3C_6H_5O_7$ (38.8 mM) solution was added to the above solution. The solution color changes from yellow to wine red by adding the $Na_3C_6H_5O_7$ solution. Magnetic stirring of blend was remained until wine red color was constant. Then, Au NPs and Cys A (1:100 volume ratio) was stirred for

approximately 12 h with steadily addition of Cys A for functionalizing citrate capped-Au NPs with Cys A. The latest color of Cys A-Au NPs mixture is deep-red color and it is stable at 4 °C up to 2 months.

2.4. Synthesis and conductivity study of ink

2.4.1. Synthesis of Ag/RGO nano-ink

GO was synthesized according to our pervious works [21,34,35]. To synthesize the nano-ink, 2.5 ml of diluted GO (graphene oxide) aqueous dispersion heated in water bath at 60 °C was added into PVP K-30 (0.5 g). The compound was magnetically stirred until complete dissolving of PVP powder into transparent and clear solution. Then, 750 μl of 0.2 mM $AgNO_3$ aqueous solution was added into above solution and magnetically stirred a minimum of 5 min in order to assure efficient blending of graphene oxide and Ag+. Later, the mixed solution kept for 12 h at 60 °C in incubator without agitation. After 12 h the solution was heated at 80 °C and magnetically stirred again. Finally, 500 μl of 8 M sodium hydroxide (NaOH) solution was drop-wisely added for increasing reduction influence. The product centrifuged at 8000 rpm for 30 min and washed 3 times with distilled water (DW) to remove extra reactant. For producing hybrid conductive nano-ink, the achieved Ag/RGO nano-ink were dispersed into EG, DW, and ethanol with volume ratio of 2.5:11.25:11.25, sonication for 30 min that led to production of water-based ink. After one day of ink maintenance for completing the reactions, the water-based ink centrifuged at 5500 rpm for 25 min and the attained pellet utilized for fabricating Ag/RGO paper-based electrode.

2.4.2. Conductivity analysis of Ag/RGO composite nano-ink

In this regard, different variety of conductive patterns designed on the photographic sheets surface through Ag/RGO pellet with various thicknesses. As represented in Fig. 1, various types of conducting patterns and a 3.0 V dip LED and 3.0 V battery was fabricated on paper substrate (for spiral conductive pattern 15.0 V battery was employed). The cathode leg of LED was linked to battery anode and so cathode surface of battery connected to one side of conductive pattern. Once the anode leg of LED touched to other side of conductive pattern, the electronic circuit switched on and the LED was lighted up. The resistance of conductive patterns including; spiral and straight lines was 0.621 MΩ and 0.012 MΩ, respectively. Also, the conductivity measurements obtained 190 μs for Ag/RGO nano-ink. For demonstrating flexibility and reliability of conductive patterns, they bended outwards by 90°. Videos about conductivity studies of patterns drawn with ink are presented in the supporting data (see supporting information).

2.5. Characterizations

2.5.1. Characterization of Au NPs and CysA/Au NPs

The shape and size of the CysA-Au NPs were evaluated by transmission electron microscope (TEM) and FE-SEM (Figs. S1 and S2 (see supporting information)). The images exhibited that the spiral shaped particles for both Au NPs and CysA/Au NPs. In spite of the secondary functionalization of Au nanoparticles, the spiral shape is preserved while a small increase in the Au NPs size could be observed. AFM images were supplied 3-dimensional structural information about CysA-Au NPs (Fig. S3 (see supporting information)). The Au NPs hydrodynamic particle sizes examined by DLS where the sizes were 20 nm. Also, Zeta potential examination of Au NPs was studied and the zeta potential value was −29.1 mV. FTIR spectroscopy was applied for evaluating the surface functional groups of Au NPs and Au NPs/CysA. As shown in Fig. S4 (see supporting information), the primary peaks of the Au NPs, Au NPs/CysA are located at 3 wave number of Au NPs, 3447, 2359 and 1653, which O—H, C—O and C═O functional groups. The N—H and C═O were located at 3500 and 1630–1690 cm^{-1} which are finger print peak of amide bond formation.

Spectrofluorometric and spectrophotometric spectra of Au NPs and corresponding images of CysA/Au NPs are exposed in Fig. S5 (see supporting information). As shown in Fig. S5A (see supporting information), bare Au NPs has an absorption peak at about 320 nm. Fig. S5B (see supporting information) indicated the Au NPs emit fluorescence signal at 580 nm but thanks to the low quantum yields, the Au NPs were not further employed in sensing applications.

2.5.2. Characterization of Ag-RGO/CysA-Au NPs, bulk Ag/RGO nano-ink, and fabricated Ag/RGO paper electrode

TEM images were recorded to evaluate the Ag/RGO nano-ink synthesis mechanism and confirm the binding of Ag NPs onto RGO (reduced graphene oxide) nano-sheets (Fig. 2). It was clearly exhibited that the abundant dispersed spherical Ag nanoparticles were decorated the RGO (reduced graphene oxide) sheets. Plentiful crystal nuclei were produced immediately when Ag NPs were added into mixture of nano-ink. PVP was absorbed onto the nuclei immediately at this moment and played as a mild reluctant, hence impede aggregation and merger of nuclei into irregular and larger NPs (Scheme 1).

Fig. 3, indicates the FE-SEM images of bulk Ag/RGO nano-ink, fabricated Ag/RGO paper electrode and CysA/Au NP modified Ag/RGO paper electrode (CysA/Au NP-Ag/RGO) to study the surface morphology. The bulk Ag/RGO nano-ink images indicated that Ag NPs with spherical uniform structure and small size decorated the RGO sheets.

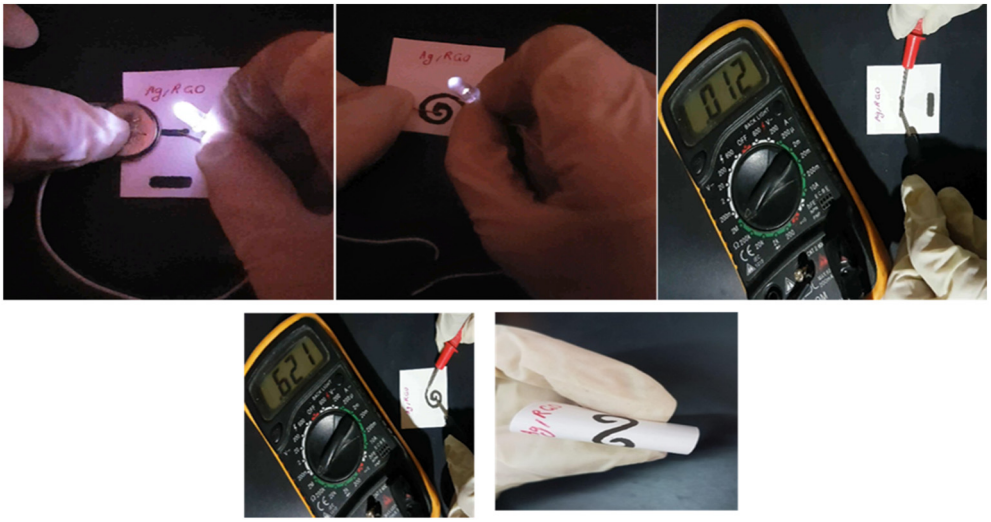

Fig. 1. Photographic images of various patterns with different thicknesses and shapes obtained by Ag/RGO nano-ink on photo paper.

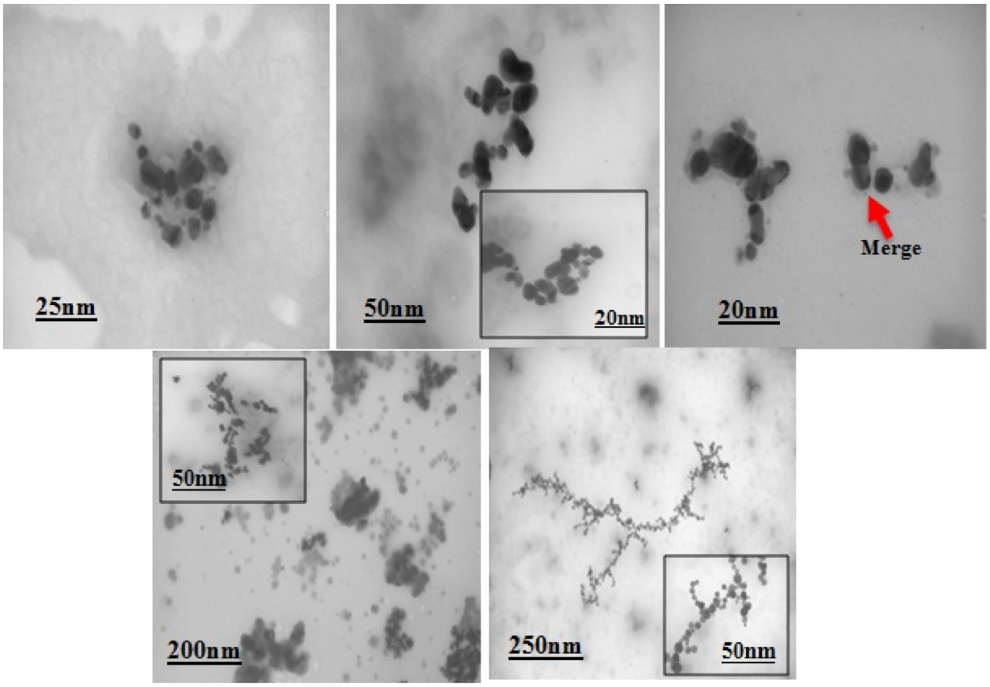

Fig. 2. TEM images of Ag/RGO nano-ink with 12 h reaction time in different nano-scales.

Ag/RGO nano-ink which was prepared in water/ethanol/EG demonstrates no aggregation of nanoparticles. When Ag/RGO nano-ink was employed to draw patterns on the photographic papers surface, it stuck to the surface of paper, aggregate randomly. According to the standard colloids theory, the colloid stability was monitored by the balance between van der Waals interaction and charged particles Coulombic repulsion [36]. It should be noted that PVP as a reducing agent has a significant effect on the alteration of Ag/RGO nano-ink conductivity because of anchoring of Ag NPs onto graphitic sheets. As the reduction process continued, more and more Ag NPs anchored onto graphene oxide sheets. The FE-SEM images of Ag-RGO/CysA-Au NPs on the photographic paper surface also show spherical particles with uniform structure, it is clear that, CysA/Au NPs were actually assembled onto the Ag/RGO surface with interaction of hydroxyl and carboxyl functional groups. Interestingly, more dispersed and less aggregated CysA/Au NPs are seen upon electrostatic interaction of Ag/RGO with CysA/Au NPs. Possibly the binding of positively charged CysA/Au NPs to the negatively charged Ag/RGO reduced the aggregation of NPs through steric hindrance.

As demonstrated in Fig. 4, signals of N and S were only related to Cys A, while signals of O, C, and N elements were related to both graphene oxide and Cys A. The large and sharp C and Ag C peaks were the usual signal for bulk C and Ag elements in the Ag/RGO nano-ink (Fig. 4A). The corresponding EDS spectra of Ag/RGO nano-ink fabricated on the paper surface and Ag-RGO/CysA-Au NPs fabricated on the paper (Fig. 4B&C) displayed the increment of Ag peak, which exhibited the deposition of nano-size silver layer along with RGO. Also, in the case of Ag-RGO/CysA-Au NP (Fig. 4C) indicated that Au element overlapped with S element.

Zeta potential analysis of Ag/RGO nano-ink was evaluated and the obtained value was −3.55 mV. Also, the hydrodynamic particle sizes of the Ag/RGO nano-ink was also determined by DLS where the sizes were 5373 d·nm.

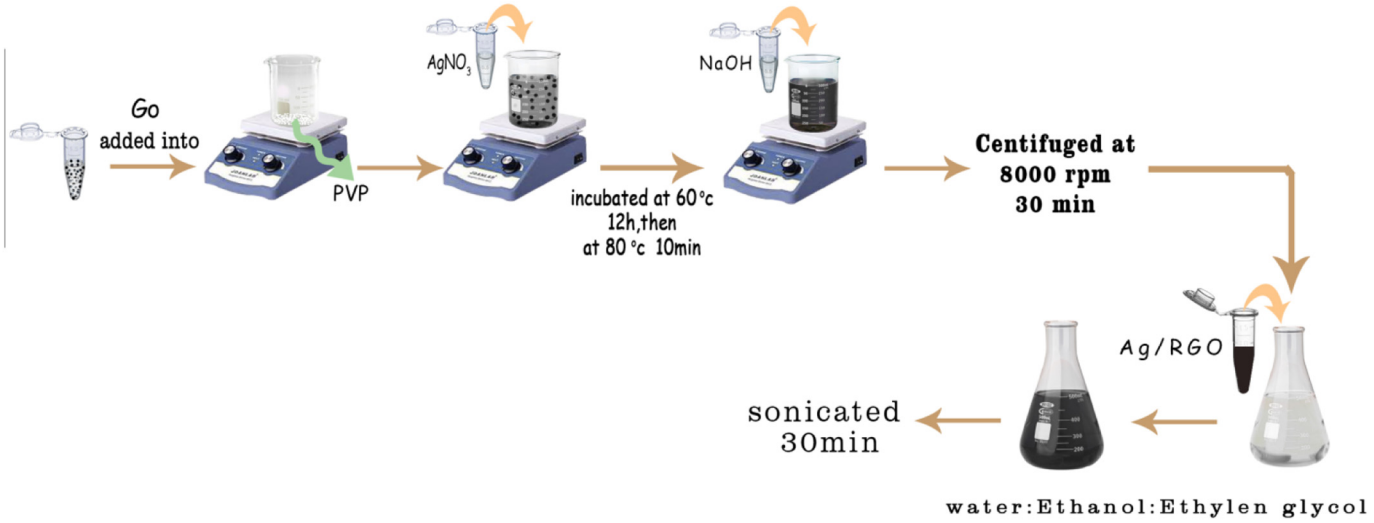

Scheme 1. Synthesis process of Ag/RGO nano-ink.

2.6. Assembly of electrochemical immunosensor

2.6.1. Ag/RGO-CysA/Au NPs paper-based electrode production

Paper is a universal substrate that has different applications science to development of microfluidic and paper based bioassays in recent years due to features such as biodegradability, availability and low cost. To prepare paper based electrode, conducting lines were drawn on the surface of the photographic paper using Ag/RGO nano-ink and for 5 min dried at room temperature. So, the prepared electrodes were treated with vaporous of hydrazine hydrate and then in order to

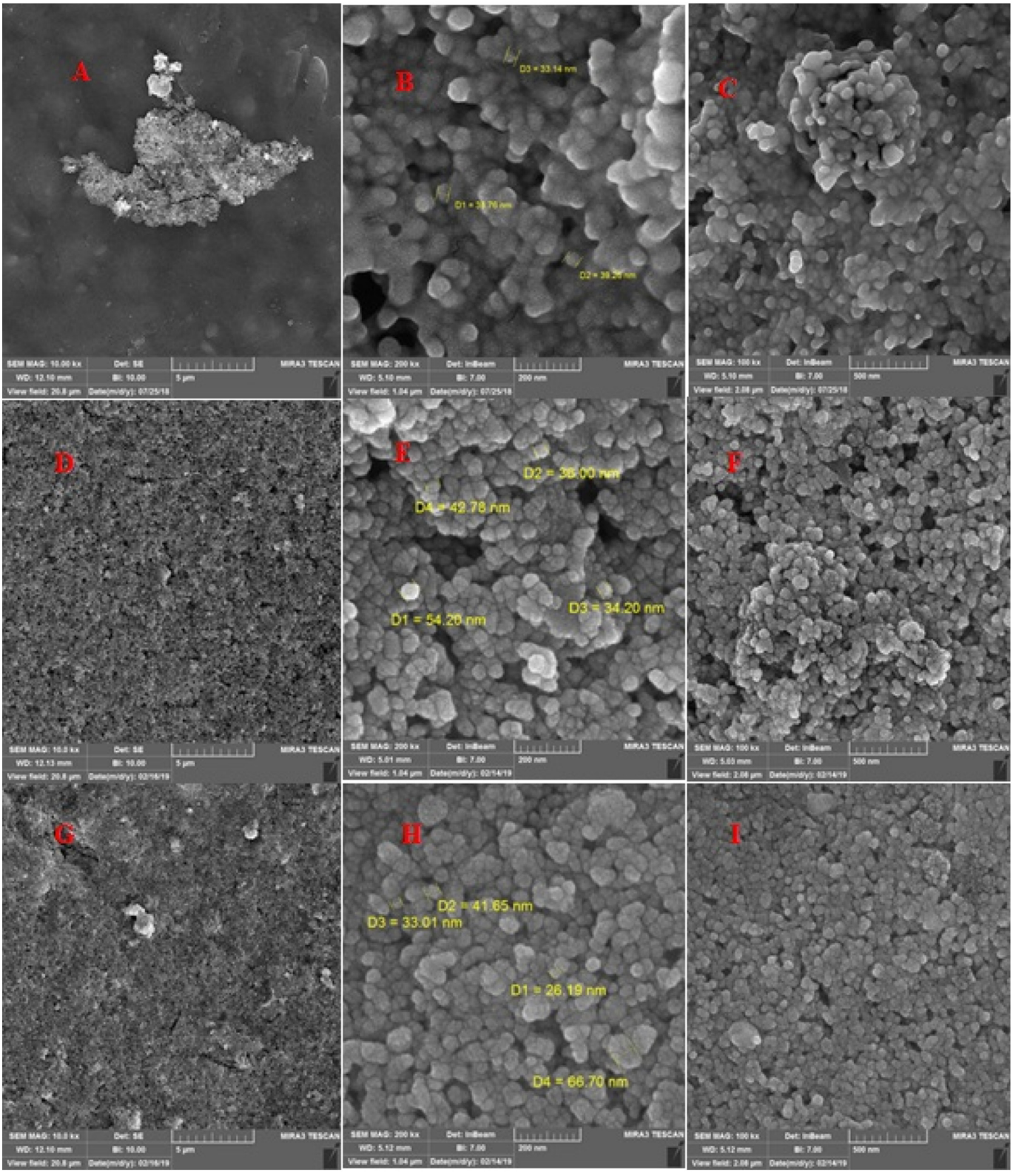

Fig. 3. (A to C) FE-SEM images of the bulk Ag/RGO nano-composite. (D to F) FE-SEM images of the Ag/RGO nano-composite drawn on the surface of photographic paper. (G to I) FE-SEM images of the Ag-RGO/CysA-Au NPs produced on the surface of photographic paper.

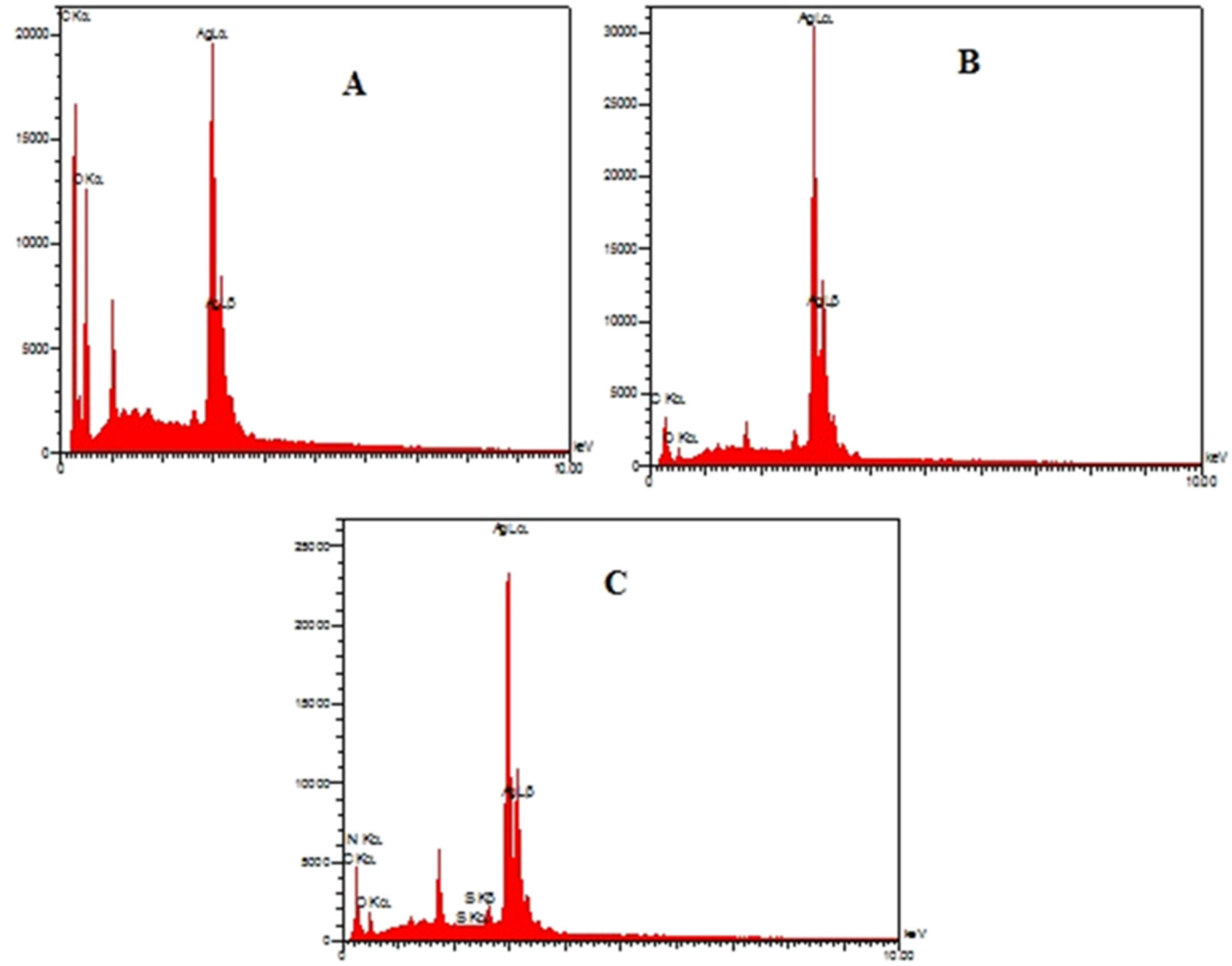

Fig. 4. EDS spectra of (A) bulk Ag/RGO nano-composite, B) Ag/RGO nano-composite drawn on the surface of photographic paper, C) Ag-RGO/CysA-Au NPs produced on the surface of photographic paper.

electrodeposition of CysA/Au NPs on the surface of Ag/RGO paper-based electrode. The fabricated electrode dipped into CysA/Au NP solution and electrodeposition was carried out by ChA technique (E = 0.8 V, duration time = 500 s) that results in attachment of NH_3 (amine) groups of CysA/Au NP with carboxyl groups of Ag/RGO paper-based electrode (Fig. 5A). Subsequently, CysA/Au NPs-Ag/RGO paper-based electrode was rinsed with distilled water in order to remove unbound moieties and maintained to dry at 25 °C.

2.6.2. Immunosensor preparation

For immunosensor design, conductive patterns were drawn on the surface of a photographic paper using Ag/RGO nano-ink. Then, 10 μl of anti-CA-125 (antibody) was activated with 0.1 M EDC and 0.4 M NHS at 4 °C for about 30 min. Then, activated antibody (20 μl) was casted onto the sensing area of CysA/Au NPs-Ag/RGO paper electrode (1 × 3 mm^2) and incubated for 3 h at 100% humidity and 4 °C. NHS/EDC leads to the activation of the fc region carboxyl group of antibody and, consequently, its covalent bond with the CysA/Au NPs-Ag/RGO paper electrode. Then 50 μg/ml of bovine serum albumin solution (blocking agent) was employed for the sites of antibody that were not bound to CysA/Au NPs-Ag/RGO paper electrode. For eliminate unbound specious, Ab-CysA/Au NPs-Ag/RGO nano-ink paper electrode cleaned with wash buffer after 1 h.

Finally, to detect the CA-125 biomarker, CA-125 antigen (10 μl) were casted onto sensing area of the engineered sensor and incubated for 1 h at 4 °C (refrigerator). Scheme 2 summarized all of the fabrications steps for the CA-125 immunosensor.

3. Results and discussion

3.1.1. Electrochemical behavior of engineered immunosensors

Ag/RGO, Ag-RGO/CysA-Au NP, Ag-RGO/CysA-Au NP/Ab, Ag-RGO/CysA-Au NP/Ab/CA 125 paper-based electrode were estimated for their electrochemical behavior in the $[Fe(CN)_6]^{3-/4-}$ solution (0.01 M). As shown in Fig. 5 (A–C), the ChAs (chronoamperograms) of the $[Fe(CN)_6]^{3-/4-}$ solution at the surface of Ag/RGO nano-ink and Ag-RGO/CysA-Au NPs modified paper-based electrode showed that application of CysA/Au NP in the fabrication of immunosensor lead to good signal amplification. Then, Au NPs were functionalized using CysA through covalent bonding between sulfur group of CysA and Au NPs [37–41]. Thereafter, CysA-Au nanoparticles provide free NH_3 group for interaction with a carboxylic group of Fc region of Ab through covalent bond [42–44]. Hence, it provides the possibility of antibody immobilization on the surface of paper-based electrode against the target analyte (cancer biomarker) and also improves the electrochemical response. After all, the biotinylated CA-125 Ab immobilization on the surface of

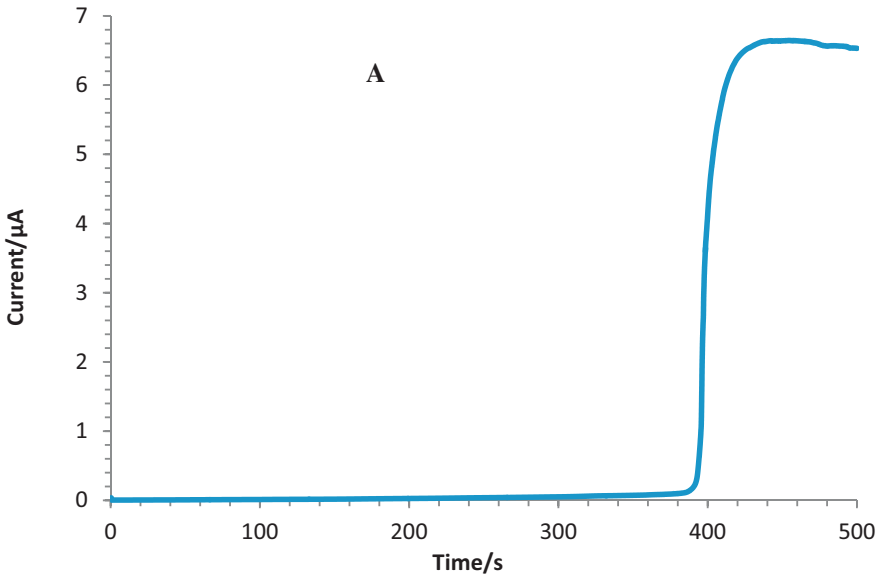
A
Current/µA
Time/s
0
1
2
3
4
5
6
7
0
100
200
300
400
500

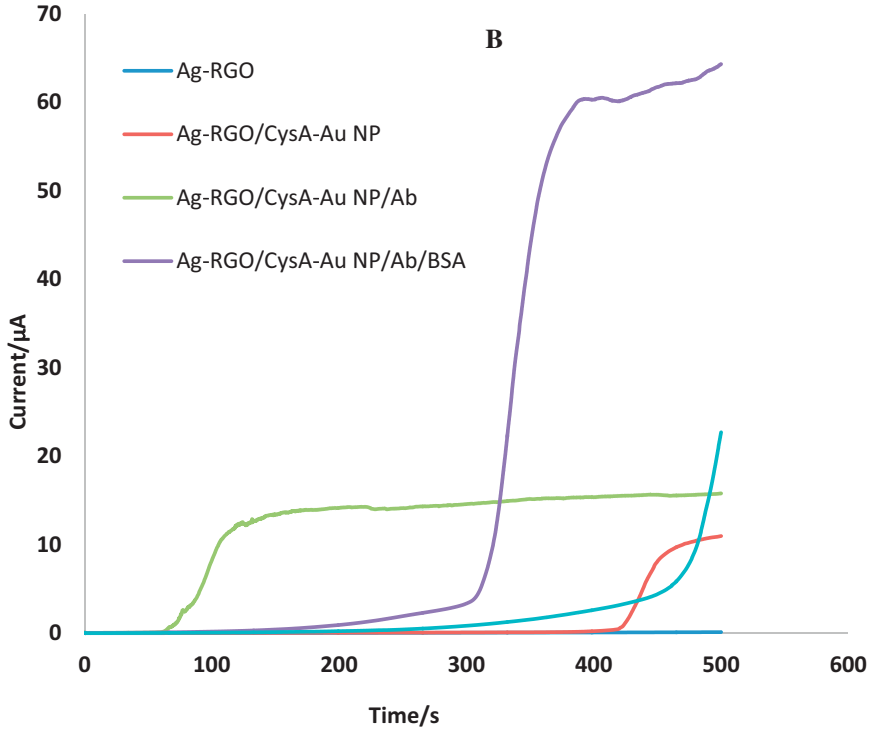
B
Ag-RGO
Ag-RGO/CysA-Au NP
Ag-RGO/CysA-Au NP/Ab
Ag-RGO/CysA-Au NP/Ab/BSA
Current/µA
Time/s
0
10
20
30
40
50
60
70
0
100
200
300
400
500
600

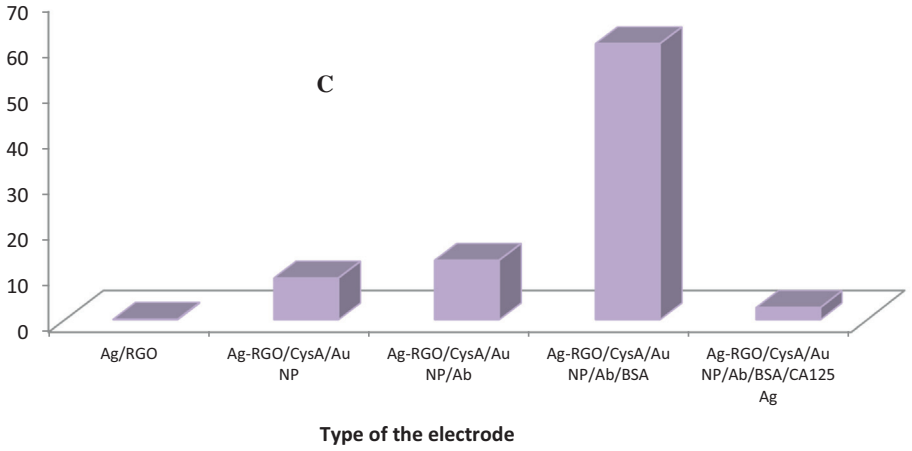
C
0
10
20
30
40
50
60
70
Ag/RGO
Ag-RGO/CysA/Au NP
Ag-RGO/CysA/Au NP/Ab
Ag-RGO/CysA/Au NP/Ab/BSA
Ag-RGO/CysA/Au NP/Ab/BSA/CA125 Ag
Type of the electrode

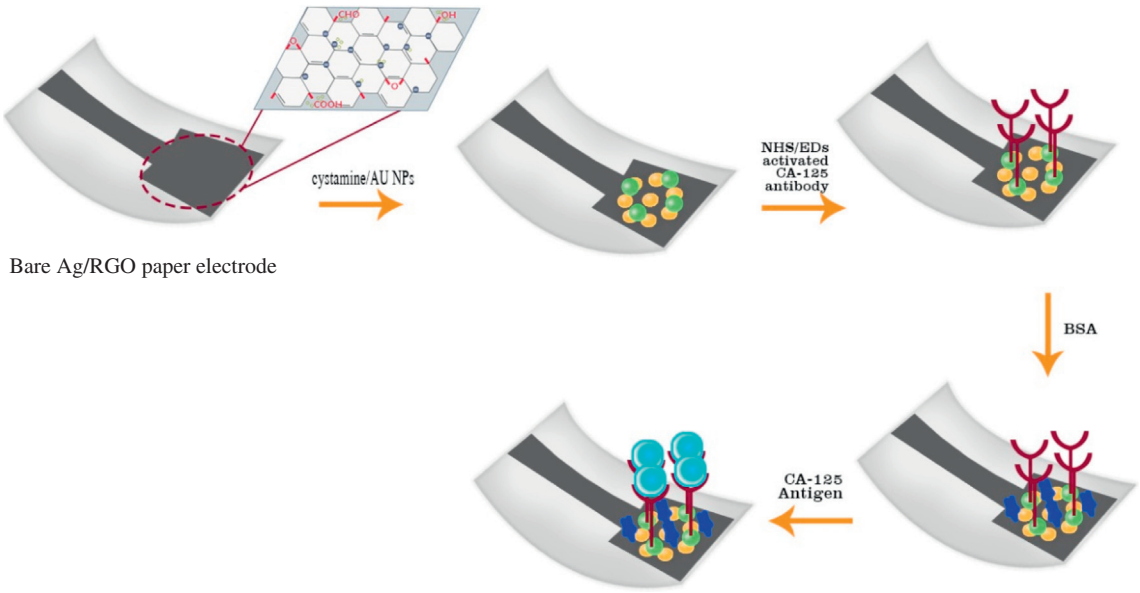

Scheme 2. Fabrication of paper based immunosensor for the detection of CA 125 biomarker.

Ag-RGO/CysA-Au NPs electrode lead to a more visibility of the peak with low current due to Ag-RGO/CysA-Au NPs interaction with Ab. But blocking using BSA leads to increase in peak currents (Fig. 5B). A remarkable decrease in peak current was seen after CA-125 antigen immobilization on the surface of electrode, which indicates that CA-125 has been immobilized favourably on the surface of Ag-RGO/CysA Au NP/Anti CA-125 paper electrode (Fig. 5C).

3.2. Analytical performance

Considering the more sensitive chronoamperometry technique than cyclic voltammetry, it can be used to study current changes over time. Therefore, this electrochemical technique was used to detect and determine CA 125 in standard and human plasma samples. For this purpose, Ag-RGO/CysA-Au NPs/Anti CA 125/BSA/Ag was incubated in different concentrations of CA 125 Ag for CA 125 electrochemical analysis. To remove antigens that were not interaction with antibody, the immunosensors prepared were rinsed completely with 0.1% Tween-PBS (pH 7.4) before electrochemical evaluations. Under optimum conditions, ChAs of Ag-RGO/CysA Au NPs/Anti CA 125/BSA/CA 125 Ag were recorded and calibration curves were obtained (Fig. 6). The results showed that, with increasing the concentration of Ag from 0 to 200 U/ml, peak current increases in regular form (Fig. 6B) which the linear range was 0.78 U/ml–400 U/ml. Also the low limit of quantification (LLOQ) was 0.78 U/ml.

The comparison of Ag-RGO/CysA-Au NPs/Anti CA 125/BSA/antigen with other modified electrodes [13,14,45–55] for CA 125 detection is shown in Table 1. According to the results obtained, it can be said that the supplied immunoassay has excellent electrical conductivity, high stability, appropriate surface area and ability to react with a biological component. Therefore, this immunoassay can be used as a suitable platform for detecting CA-125 in biological samples.

3.3. Real sample analysis

According to the results, proposed method can also be used toward detection and determination of CA 125 biomarker in the human plasma

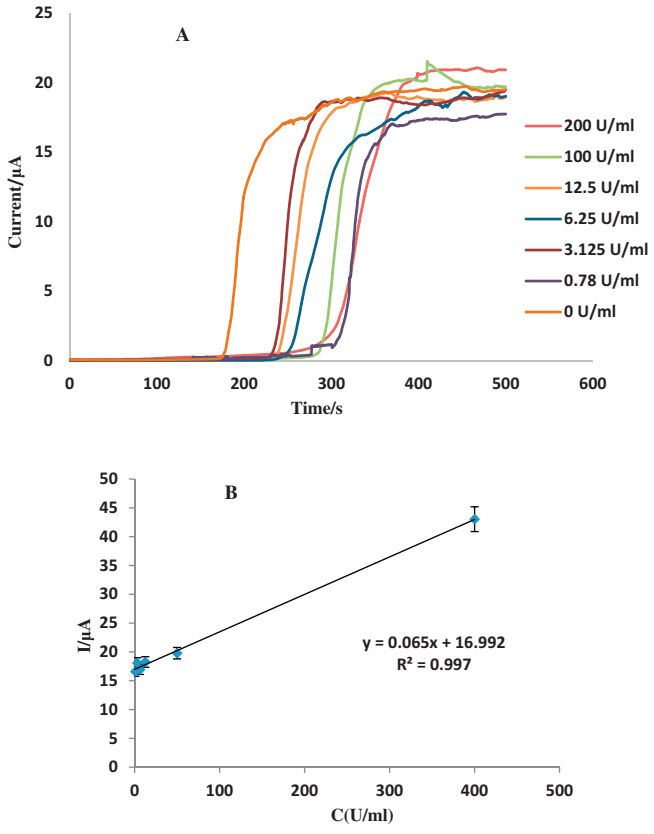

Fig. 6. A) ChAs obtained for determination of different concentrations of CA 125 Ag (0.78, 3.125, 6.25, 12.5, 100, 200 U/ml) using Ag-RGO/CysA-Au NP/Ab/BSA in 0.01 M $[Fe(CN)6]^{3-/4-}$, KCl. ChA parameters: E = 0.0 V and record time of 500 s. B) Calibration curves of CA 125 biomarker.

Fig. 5. A) ChAs for the electrochemical deposition of CysA/Au NP on the surface of Ag/RGO paper-based electrode. E = 0.0 V vs. Ag/AgCl and the duration time was 500 s. B) ChAs of Ag-RGO, Ag-RGO/CysA-Au NP, Ag-RGO/CysA-Au NP/Ab, Ag-RGO/CysA-Au NP/Ab/BSA, Ag-RGO/CysA-Au NP/Ab/BSA/CA125 Ag paper electrode in 0.01 M $[Fe(CN)_6]^{3-/4-}$, KCl. ChA parameters: E = 0.0 V and record time of 500 s. C) Histogram of the peak currents obtained from the electrode preparation steps.

Table 1
A comparison of the performance of diverse immunosensors for CA 125 detection.

Assay strategy	Signal amplification	LOD (U/ml)	Ref.
Electrochemical immunosensor	Ag-GQDs nano ink	0.01 U/ml	[45]
Ultrasensitive immunoassay	Au NPs	0.1 U/ml	[13]
Surface plasmon resonance capacitor immunosensors label free		0.1 U/ml	[46]
Impedometric immunosensor	(AuNPs@SiO_2), Cdse QD	0.0016 U/ml	[47]
Fluorescence labeling, imaging and sensing	Green and economic carbon dots	3 × 10–7 U/ml	[48]
Electrochemistry of HRP	HRP	1.29 U/ml	[49]
Chemiluminescence	GQD	0.05 U/ml	[50]
Electrochemical immunosensor	Zno nanorods-Au nanoparticles	0.0015 U/ml	[51]
Fluorescence-free	Plasmonic scattering based	0.0018 U/ml	[52]
Aptamer and 5-fluorouraci	Ag_2S quantum dots	0.042 U/ml	[53]
Immunoassay	Ag@Co_3O_4 nanosheets	0.00015 U/ml	[54]
Amperometric immunosensor for separation-free	Thionin on carbon nanofiber	1.8 U/ml	[55]
Electrochemical immunosensor	P(CTAB-CS)-Ag NPs	0.001 U/ml	[14]
Electrochemical immunosensor	Ag-RGO/CysA-Au NPs	0.78 U/ml	This work

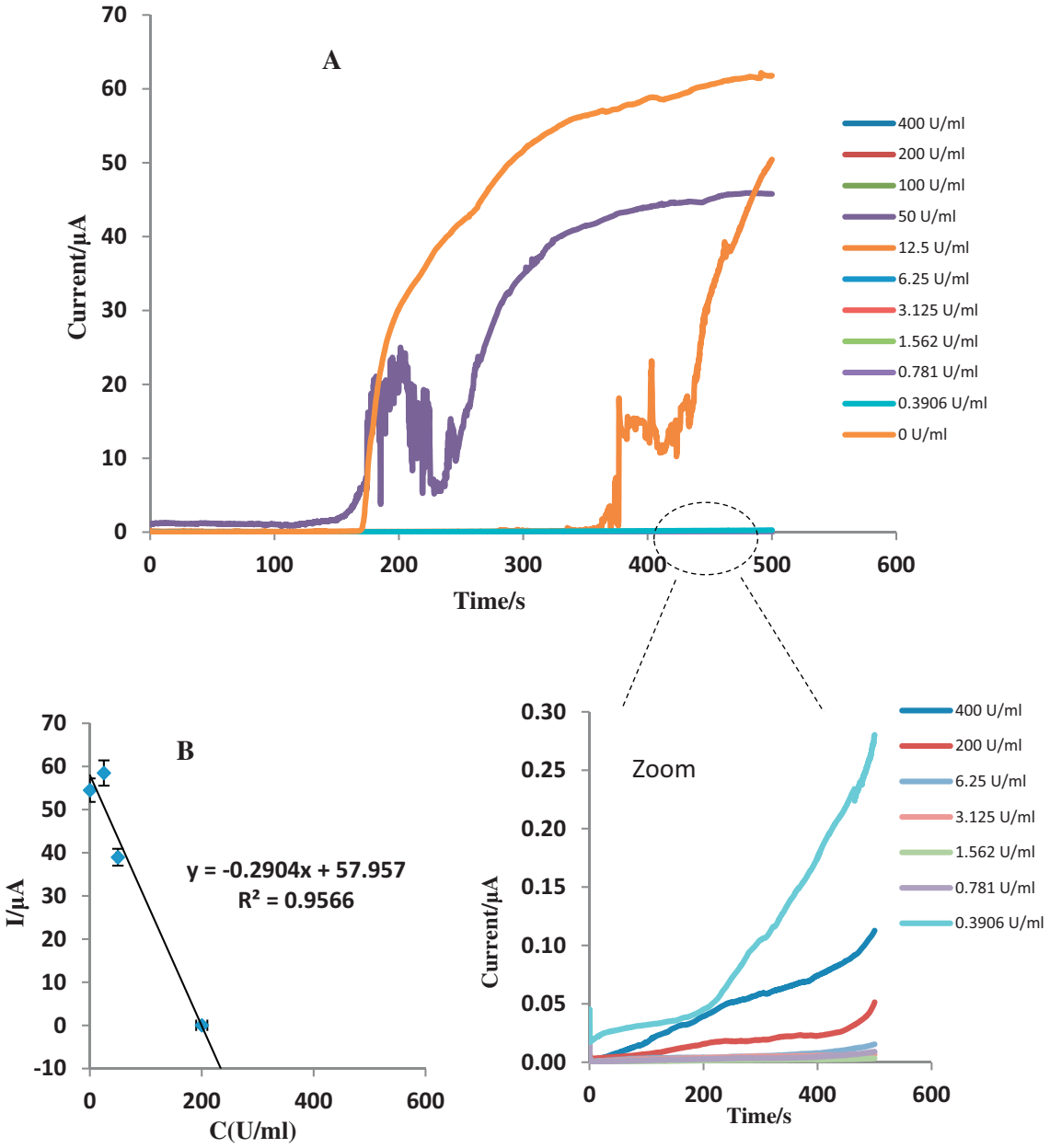

Fig. 7. A) ChAs obtained Ag-RGO/CysA-Au NP/Ab/BSA for determination of different concentrations of antigen (0, 0.39, 0.78, 1.56, 3.125, 6.25, 12.5, 50, 100, 200, 400 U/ml) in human plasma samples using Ag-RGO/CysA-Au NP/Ab/BSA in 0.01 M $[Fe(CN)_6]^{3-/4-}$, KCl. ChA parameters: E = 0.0 V and record time of 500 s. B) Calibration curves of the Ag-RGO/CysA-Au NPs/Anti CA125 (Ab)/BSA/CA125 antigen paper electrode in presence of plasma.

samples using ChA technique (Fig. 7). As mentioned erstwhile, the 0.01 M $[Fe(CN)_6]^{3-/4-}$, KCl (pH 7.4) was elected as the support electrolyte for the measurement of CA 125. For this intent, 10 μl of unprocessed human plasma were mixed with 10 μl of various concentrations of CA-125 Ag, casted onto the sensing of CA-125. In optimum conditions, the calibration curve was obtained by plotting the peak current against the mixture of CA-125 Ag and plasma concentration (Fig. 7B). Using ChA technique, the dynamic range was 0.78 to 200 U/ml and LLOQ (low limits of quantitation) was 0.78 U/ml.

3.4. Stability and reproducibility

Stability and reproducibility are two significant factors that are to evaluate the performance of the sensor. The stability of the paper-sensor prepared by measuring the decrease in the intensity of the current during repeatable ChA measured with Ag-RGO/CysA/Au NPs paper-electrodes. To examine the inter-electrode reproducibility of Ag-RGO/CysA/Au NPs paper-electrode, three modified electrodes were studied simultaneously by recording ChAs in 0.01 M solution of $[Fe(CN)_6]^{3-/4-}$. Also, the intraday stability of the Ag-RGO/CysA-Au NPs paper-electrode was investigated by measuring the variation of current for about 6 days by storing the electrode in dark condition for 6 days and testing by chronoamperometry techniques. The results showed that the electrodes are not stable in different days, which can be concluded that this sensor offers better performance on the day it prepares.

Apart from the electrochemical sensing, the change of fluorescence intensity of biomolecules for sensing and imaging should be another important and interest tool. For example, the dyes with aggregation-induced emission (AIE) feature have been extensively utilized for sensing and biological imaging applications [56–67].

4. Conclusion

In summary, a reliable, rapid and effective paper based biodevice was developed for the detection of CA 125. Easy handwriting method using conductive nano-composite to prepare paper electrode was employed in this strategy. A new platform (based on Ag/RGO nano-ink) built on the surface of photographic paper was employed to sensitive detection of CA-125 cancer biomarker with application of CysA/Au NPs (signal amplification). CysA/Au NPs were covalently bonded to Ag/RGO on the paper surface and employed to immobilization of anti-CA 125 Ab. Experimental results shown that engineered immunoassay can effectively improve electron transfer efficacy based on synergetic effect of CysA/Au NPs on conductive surface (Ag/RGO). In optimum conditions, the immunosensor displayed linear range of 0.78–400 U/ml and with LLOQ of 0.78 U/ml. The engineered immunosensor showed great analytical performance for detection of CA-125. Also, the designed immunosensor can determine CA-125 in human plasma sample. According to the results, this can be concluding that this platform promisingly has the potential to be employed in diagnosis of ovarian cancer as a simple and appropriate assay.

Acknowledgment

Research reported in this publication was supported by Elite Researcher Grant Committee under award number [982534] from the National Institute for Medical Research Development (NIMAD), Tehran, Iran. Also, we thank Tabriz University of Medical Sciences for instrumental supporting of this research.

Appendix A. Supplementary data

Supplementary data to this article can be found online at https://doi.org/10.1016/j.ijbiomac.2019.07.109.

References

[1] M. Matz, M.P. Coleman, M. Sant, M.D. Chirlaque, O. Visser, M. Gore, C. Allemani, S. Bouzbid, M. Hamdi-Chérif, Z. Zaidi, The histology of ovarian cancer: worldwide distribution and implications for international survival comparisons (CONCORD-2), Gynecol. Oncol. 144 (2) (2017) 405–413.
[2] F.R. Nezhat, R. Apostol, C. Nezhat, T. Pejovic, New insights in the pathophysiology of ovarian cancer and implications for screening and prevention, Am. J. Obstet. Gynecol. 213 (3) (2015) 262–267.
[3] R.J. Kurman, Origin and molecular pathogenesis of ovarian high-grade serous carcinoma, Ann. Oncol. 24 (suppl_10) (2013) x16–x21.
[4] B.V. Chikkaveeraiah, A.A. Bhirde, N.Y. Morgan, H.S. Eden, X. Chen, Electrochemical immunosensors for detection of cancer protein biomarkers, ACS Nano 6 (8) (2012) 6546–6561.
[5] H.-J. Song, J.-K. Yim, C.-Y. Park, Y.-S. Kim, J.-D. Kim, Comparison of the diagnostic performances of CA125 and multiple marker combinations for early diagnosis of ovarian cancer, Int. J. Biosci. Biotech. 5 (5) (2013) 141–150.
[6] E. Høgdall, Cancer antigen 125 and prognosis, Curr. Opin. Obstet. Gynecol. 20 (1) (2008) 4–8.
[7] R.C. Bast, M. Feeney, H. Lazarus, L. Nadler, R. Colvin, R. Knapp, Reactivity of a monoclonal antibody with human ovarian carcinoma, J. Clin. Invest. 68 (5) (1981) 1331–1337.
[8] D. Gupta, C.G. Lis, Role of CA125 in predicting ovarian cancer survival-a review of the epidemiological literature, J. Ovarian Res. 2 (1) (2009) 13.
[9] V.A. Moyer, Screening for ovarian cancer: US preventive services task force reaffirmation recommendation statement, Ann. Intern. Med. 157 (12) (2012) 900–904.
[10] N. Razmi, M. Hasanzadeh, Current advancement on diagnosis of ovarian cancer using biosensing of CA 125 biomarker: analytical approaches, Trends Anal. Chem. 108 (2018) 1–12.
[11] X. Zheng, S. Chen, L. Li, X. Liu, X. Liu, S. Dai, P. Zhang, H. Lu, Z. Lin, Y. Yu, Evaluation of HE4 and TTR for diagnosis of ovarian cancer: comparison with CA-125, J. Gynaecol. Obstet. Hum. Reprod. 47 (6) (2018) 227–230.
[12] P. Hohlfeld, T.T. Dang, K. Nahoul, F. Daffos, F. Forestier, Tumour-associated antigens in maternal and fetal blood, Prenat. Diagn. 14 (10) (1994) 907–912.
[13] M. Hasanzadeh, R. Sahmani, E. Solhi, A. Mokhtarzadeh, N. Shadjou, S. Mahboob, Ultrasensitive immunoassay of carcinoma antigen 125 in untreated human plasma samples using gold nanoparticles with flower like morphology: a new platform in early stage diagnosis of ovarian cancer and efficient management, Int. J. Biol. Macromol. 119 (2018) 913–925.
[14] M. Hasanzadeh, A. Mohammadzadeh, M. Jafari, B. Habibi, Ultrasensitive immunoassay of glycoprotein 125 (CA 125) in untreated human plasma samples using poly (CTAB-chitosan) doped with silver nanoparticles, Int. J. Biol. Macromol. 120 (2018) 2048–2064.
[15] M. Jafari, M. Hasanzadeh, E. Solhi, S. Hassanpour, N. Shadjou, A. Mokhtarzadeh, A. Jouyban, S. Mahboob, Ultrasensitive bioassay of epitope of Mucin-16 protein (CA 125) in human plasma samples by using of novel immunoassay: a new platform in early stage diagnosis of ovarian cancer and efficient management, Int. J. Biol. Macromol. 126 (2019) 1255–1265.
[16] M. Hasanzadeh, S. Tagi, E. Solhi, N. Shadjou, A. Jouyban, A. Mokhtarzadeh, Immunosensing of breast cancer prognostic marker in adenocarcinoma cell lysates and unprocessed human plasma samples using gold nanostructure coated on organic substrate, Int. J. Biol. Macromol. 118 (2018) 1082–1089 Pt A.
[17] M. Hasanzadeh, S. Tagi, E. Solhi, A. Mokhtarzadeh, N. Shadjou, A. Eftekhari, S. Mahboob, An innovative immunosensor for ultrasensitive detection of breast cancer specific carbohydrate (CA 15-3) in unprocessed human plasma and MCF-7 breast cancer cell lysates using gold nanospear electrochemically assembled onto thiolated graphene quantum dots, Int. J. Biol. Macromol. 114 (2018) 1008–1017.
[18] M. Hasanzadeh, E. Solhi, M. Jafari, A. Mokhtarzadeh, J. Soleymani, A. Jouyban, S. Mahboob, Ultrasensitive immunoassay of tumor protein CA 15.3 in MCF-7 breast cancer cell lysates and unprocessed human plasma using gold nanoparticles doped on the structure of mesoporous silica, Int. J. Biol. Macromol. 120 (2018) 2493–2508.
[19] H. Ashrafi, M. Hasanzadeh, K. Ansarin, SA. Ozkan, A. Jouyban, Application of chitosan as biocompatible polysaccharide in quantification of some benzodiazepines affecting sleep disorders: A new platform for preparation of bioactive scaffolds, Int. J. Biol. Macromol. 120 (2018) 2466–2481.
[20] H. Malekzad, M. Hasanzadeh, N. Shadjou, A. Jouyban, Highly sensitive immunosensing of prostate specific antigen using poly cysteine caped by graphene quantum dots and gold nanoparticle: a novel signal amplification strategy, Int. J. Biol. Macromol. 105 (2017) 522–532.
[21] L. Saghatforoush, M. Hasanzadeh, N. Shadjou, Polystyrene–graphene oxide modified glassy carbon electrode as a new class of polymeric nanosensors for electrochemical determination of histamine, Chin. Chem. Lett. 25 (4) (2014) 655–658.
[22] M. Hasanzadeh, N. Shadjou, (Fe_3O_4)–graphene oxide–SO_3H as a new magnetic nanocatalyst for electro-oxidation and determination of selected parabens, J. Nanosci. Nanotechnol. 13 (7) (2013) 4909–4916.
[23] M. Hasanzadeh, HN. Baghban, N. Shadjou, Non-enzymatic determination of L-Proline amino acid in unprocessed human plasma sample using hybrid of graphene quantum dots decorated with gold nanoparticles and poly cysteine: a novel signal amplification strategy, Anal. Sci. 34 (3) (2018) 355–362.
[24] M. Hasanzadeh, N. Shadjou, Y. Lin, M. de la Guardia, Nanomaterials for use in immunosensing of carcinoembryonic antigen (CEA): recent advances, TrAC Trends Anal. Chem. 86 (2017) 185–205.
[25] R. Duan, X. Zhou, D. Xing, Electrochemiluminescence biobarcode method based on cysteamine−gold nanoparticle conjugates, Anal. Chem. 82 (8) (2010) 3099–3103.

[26] T. Mazzu-Nascimento, G.G. Morbioli, L.A. Milan, F.C. Donofrio, C.A. Mestriner, E. Carrilho, Development and statistical assessment of a paper-based immunoassay for detection of tumor markers, Anal. Chim. Acta 950 (2017) 156–161.
[27] S. Hassanpour, A. Saadati, M. Hasanzadeh, N. Shadjou, A. Mirzaie, A. Jouyban, Direct writing of biocatalytic materials based on pens filled with high-tech enzymatic inks: "Do-it-Yourself", Microchem. J. 145 (2019) 266–272.
[28] Z. Liu, J. Hu, Z. Qu, F. Xu, Based immunoassays, Handbook of Immunoassay Technologies, Elsevier 2018, pp. 183–201.
[29] X. Li, D.R. Ballerini, W. Shen, A perspective on paper-based microfluidics: current status and future trends, Biomicrofluidics 6 (1) (2012), 011301.
[30] S.K. Mahadeva, K. Walus, B. Stoeber, Paper as a platform for sensing applications and other devices: a review, ACS Appl. Mater. Interfaces 7 (16) (2015) 8345–8362.
[31] S. Hassanpour, M. Hasanzadeh, A. Saadati, N. Shadjou, J. Soleymani, A. Jouyban, A novel paper based immunoassay of breast cancer specific carbohydrate (CA 15.3) using silver nanoparticles-reduced graphene oxide nano-ink technology: a new platform to construction of microfluidic paper-based analytical devices (μPADs) towards biomedical analysis, Microchem. J. 146 (2019) 345–358.
[32] F.A.a. Alatraktchi, J.S. Noori, G.P. Tanev, J. Mortensen, M. Dimaki, H.K. Johansen, J. Madsen, S. Molin, W.E. Svendsen, Based sensors for rapid detection of virulence factor produced by Pseudomonas aeruginosa, PLoS One 13 (3) (2018), e0194157.
[33] A. Russo, B.Y. Ahn, J.J. Adams, E.B. Duoss, J.T. Bernhard, J.A. Lewis, Pen-on-paper flexible electronics, Adv. Mater. 23 (30) (2011) 3426–3430.
[34] L. Saghatforoush, M. Hasanzadeh, N. Shadjou, ß-Cyclodextrin/graphene oxide grafted sulfonic acid: application for electro-oxidation and determination of cadaverine in fish samples, J. Electroanal. Chem. 714 (2014) 79–84.
[35] M. Hasanzadeh, M.H. Pournaghi-Azar, N. Shadjou, A. Jouyban, A new mechanistic approach to elucidate furosemide electrooxidation on magnetic nanoparticles loaded on graphene oxide modified glassy carbon electrode, RSC Adv. 4 (13) (2014) 6580–6590.
[36] S. Wang, H. Xin, Fractal and dendritic growth of metallic ag aggregated from different kinds of γ-irradiated solutions, J. Phys. Chem. B 104 (24) (2000) 5681–5685.
[37] P.D. Jadzinsky, G. Calero, C.J. Ackerson, D.A. Bushnell, R.D. Kornberg, Structure of a thiol monolayer-protected gold nanoparticle at 1.1 Å resolution, Science 318 (5849) (2007) 430–433.
[38] P.R. Solanki, M.K. Patel, M.A. Ali, B. Malhotra, A chitosan modified nickel oxide platform for biosensing applications, J. Mater. Chem. B 3 (32) (2015) 6698–6708.
[39] R. Polsky, R. Gill, L. Kaganovsky, I. Willner, Nucleic acid-functionalized Pt nanoparticles: catalytic labels for the amplified electrochemical detection of biomolecules, Anal. Chem. 78 (7) (2006) 2268–2271.
[40] E.E. Connor, J. Mwamuka, A. Gole, C.J. Murphy, M.D. Wyatt, Gold nanoparticles are taken up by human cells but do not cause acute cytotoxicity, Small 1 (3) (2005) 325–327.
[41] X. Luo, A. Morrin, A.J. Killard, M.R. Smyth, Application of nanoparticles in electrochemical sensors and biosensors, Electroanalysis 18 (4) (2006) 319–326.
[42] M. Hasanzadeh, N. Shadjou, A. Mokhtarzadeh, M. Ramezani, Two dimension (2-D) graphene-based nanomaterials as signal amplification elements in electrochemical microfluidic immune-devices: recent advances, Mater. Sci. Eng. C 68 (2016) 482–493.
[43] M. Hasanzadeh, N. Razmi, A. Mokhtarzadeh, N. Shadjou, S. Mahboob, Aptamer based assay of plated-derived grow factor in unprocessed human plasma sample and MCF-7 breast cancer cell lysates using gold nanoparticle supported α-cyclodextrin, Int. J. Biol. Macromol. 108 (2018) 69–80.
[44] M. Hasanzadeh, N. Shadjou, M. Marandi, Graphene quantum dot functionalized by chitosan and beta-cyclodextrin as a new support nanocomposite material for efficient methanol electrooxidation, J. Alloys Compd. 688 (2016) 171–186.
[45] M. Jafari, M. Hasanzadeh, E. Solhi, S. Hassanpour, N. Shadjou, A. Mokhtarzadeh, A. Jouyban, S. Mahboob, Ultrasensitive bioassay of epitope of Mucin-16 protein (CA 125) in human plasma samples using a novel immunoassay based on silver conductive nano-ink: a new platform in early stage diagnosis of ovarian cancer and efficient management, Int. J. Biol. Macromol. 126 (2019) 1255–1265.
[46] S. Suwansa-ard, P. Kanatharana, P. Asawatreratanakul, B. Wongkittisuksa, C. Limsakul, P. Thavarungkul, Comparison of surface plasmon resonance and capacitive immunosensors for cancer antigen 125 detection in human serum samples, Biosens. Bioelectron. 24 (12) (2009) 3436–3441.
[47] M. Johari-Ahar, M. Rashidi, J. Barar, M. Aghaie, D. Mohammadnejad, A. Ramazani, P. Karami, G. Coukos, Y. Omidi, An ultra-sensitive impedimetric immunosensor for detection of the serum oncomarker CA-125 in ovarian cancer patients, Nanoscale 7 (8) (2015) 3768–3779.
[48] S. Hamd-Ghadareh, A. Salimi, F. Fathi, S. Bahrami, An amplified comparative fluorescence resonance energy transfer immunosensing of CA125 tumor marker and ovarian cancer cells using green and economic carbon dots for bio-applications in labeling, imaging and sensing, Biosens. Bioelectron. 96 (2017) 308–316.
[49] Z. Dai, F. Yan, J. Chen, H. Ju, Reagentless amperometric immunosensors based on direct electrochemistry of horseradish peroxidase for determination of carcinoma antigen-125, Anal. Chem. 75 (20) (2003) 5429–5434.
[50] I. Al-Ogaidi, H. Gou, Z.P. Aguilar, S. Guo, A.K. Melconian, A.K.A. Al-Kazaz, F. Meng, N. Wu, Detection of the ovarian cancer biomarker CA-125 using chemiluminescence resonance energy transfer to graphene quantum dots, Chem. Commun. 50 (11) (2014) 1344–1346.
[51] G. Gasparotto, J.P.C. Costa, P.I. Costa, M.A. Zaghete, T. Mazon, Electrochemical immunosensor based on ZnO nanorods-au nanoparticles nanohybrids for ovarian cancer antigen CA-125 detection, Mater. Sci. Eng. C 76 (2017) 1240–1247.
[52] S.K. Chakkarapani, P. Zhang, S. Ahn, S.H. Kang, Total internal reflection plasmonic scattering-based fluorescence-free nanoimmunosensor probe for ultra-sensitive detection of cancer antigen 125, Biosens. Bioelectron. 81 (2016) 23–31.
[53] H. Jin, R. Gui, J. Gong, W. Huang, Aptamer and 5-fluorouracil dual-loading Ag_2S quantum dots used as a sensitive label-free probe for near-infrared photoluminescence turn-on detection of CA125 antigen, Biosens. Bioelectron. 92 (2017) 378–384.
[54] X. Ren, H. Wang, D. Wu, D. Fan, Y. Zhang, B. Du, Q. Wei, Ultrasensitive immunoassay for CA125 detection using acid site compound as signal and enhancer, Talanta 144 (2015) 535–541.
[55] L. Wu, F. Yan, H. Ju, An amperometric immunosensor for separation-free immunoassay of CA125 based on its covalent immobilization coupled with thionine on carbon nanofiber, J. Immunol. Methods 322 (1–2) (2007) 12–19.
[56] J. Liu, J.W.Y. Lam, B. Zhong Tang, Acetylenic polymers: syntheses, structures, and functions, Chem. Rev. 109 (2009) 5799–5867.
[57] X. Zhang, K. Wang, M. Liu, X. Zhang, L. Tao, Y. Chen, Y. Wei, Polymeric AIE-based nanoprobes for biomedical applications: recent advances and perspectives, Nanoscale 7 (2015) 11486–11508.
[58] Q. Wan, Q. Huang, M. Liu, D. Xu, X. Zhang, Y. Wei, Aggregation-induced emission active luminescent polymeric nanoparticles: non-covalent fabrication methodologies and biomedical applications, Appl. Mater. Today 9 (2017) 145–160.
[59] H. Huang, M. Liu, Q. Wan, R. iang, D. Xu, Q. Huang, Y. Wen, F. Deng, X. Zhang, Y. Wei, Facile fabrication of luminescent hyaluronic acid with aggregation-induced emission through formation of dynamic bonds and their theranostic applications, Mater. Sci. Eng. C 91 (2018) 201–207.
[60] Z. Long, L. Mao, M. Liu, Q. Wan, Y. Wan, X. Zhang, Y. Wei, Marrying multicomponent reactions and aggregation-induced emission (AIE): new directions for fluorescent nanoprobes, Polym. Chem. 8 (2017) 5644–5654.
[61] Z. Long, M. Liu, K. Wang, F. Deng, X. Zhang, Y. Wei, Facile synthesis of AIE-active amphiphilic polymers: self-assembly and biological imaging applications, Mater. Sci. Eng. C 66 (2016) 215–220.
[62] L. Huang, S. Yang, J. Chen, J. Tian, X. Zhang, Y. Wei, A facile surface modification strategy for fabrication of fluorescent silica nanoparticles with the aggregation-induced emission dye through surface-initiated cationic ring opening polymerization, Mater. Sci. Eng. C 94 (2019) 270–278.
[63] R. Jiang, M. Liu, H. Huang, L. Mao, X. Zhang, Y. Wei, Facile fabrication of organic dyed polymer nanoparticles with aggregation-induced emission using an ultrasound-assisted multicomponent reaction and their biological imaging, J. Colloid Interface Sci. 519 (2018) 137–144.
[64] Z. Long, M. Liu, R. Jiang, Q. Wan, X. Zhang, Y. Wei, Preparation of water soluble and biocompatible AIE-active fluorescent organic nanoparticles via multicomponent reaction and their biological imaging capability, Chem. Eng. J. 308 (2017) 527–534.
[65] H. Huang, M. Liu, R. Jiang, J. Chen, X. Zhang, Y. Wei, Facile modification of nanodiamonds with hyperbranched polymers based on supramolecular chemistry and their potential for drug delivery, J. Colloid Interface Sci. 513 (2018) 198–204.
[66] X. Zhang, X. Zhang, B. Yang, M. Liu, W. Liu,a Y. Chen, Y. Wei. Fabrication of aggregation induced emission dye-based fluorescent organic nanoparticles via emulsion polymerization and their cell imaging applications. Polym. Chem., 2014, 5, 399–404.
[67] X. Zhang, X. Zhang, B. Yang, M. Liu, W. Liu, Y. Chen, Y. Wei, Polymerizable aggregation-induced emission dye-based fluorescent nanoparticles for cell imaging applications, Polym. Chem. 5 (2014) 356–360.